INTERNATIONAL JOURNAL FOR NUMERICAL METHODS IN ENGINEERING
Int. J. Numer. Meth. Engng 2001; **50**:1291–1305

Embedded crack model. Part II: Combination with smeared cracks

Milan Jirásek*,† and Thomas Zimmermann

Laboratory of Structural and Continuum Mechanics, Department of Civil Engineering, Swiss Federal Institute of Technology (EPFL), CH-1015 Lausanne, Switzerland

SUMMARY

The paper investigates the behaviour of finite elements with embedded displacement discontinuities that represent cracks. Examples of fracture simulations show that an incorrect separation of nodes due to a locally mispredicted crack direction leads to a severe stress locking, which produces spurious secondary cracking. As a possible remedy the paper advocates a new concept of a model with transition from a smeared to an embedded (discrete) crack. An additional improvement is achieved by reformulating the smeared part as non-local. Various criteria for placing the discontinuity are compared, and the optimal technique is identified. Remarkable insensitivity of the resulting model to mesh-induced directional bias is demonstrated. It is shown that the transition to an explicit description of a widely opening crack as a displacement discontinuity improves the behaviour of the combined model and remedies certain pathologies exhibited by regularized continuum models. Copyright © 2001 John Wiley & Sons, Ltd.

KEY WORDS: fracture; damage; cracking; localization; embedded discontinuities; non-local continuum; stress locking

1. MULTIPLE EMBEDDED CRACKS

In Part I of this paper [1] we have developed the theoretical formulation and numerical algorithms for triangular finite elements with embedded cracks (strong discontinuities) described by a damage-type traction-separation law. These elements shall now be tested on several typical fracture problems, and the results shall be compared to those obtained with smeared crack models implemented into standard constant-strain triangular elements (CST).

As the first example, consider the three-point-bend specimen in Figure 1(a). The load–displacement diagram in Figure 1(b) and the crack patterns‡ in Figures 1(c) and 1(d) show

*Correspondence to: Milan Jirásek, Laboratory of Structural and Continuum Mechanics (LSC), Swiss Federal Institute of Technology (EPFL), CH-1015, Lausanne, Switzerland
†E-mail: Milan.Jirasek@EPFL.ch

Contract/grant sponsor: Swiss Commission for Technology and Innovation, contract/grant number: CTI-3201.1

‡In Figures 1(c) and 1(d), the thickness of lines representing cracks is proportional to the inelastic strain, in order to show which cracks dominate.

Received 9 November 1998
Revised 5 February 1999

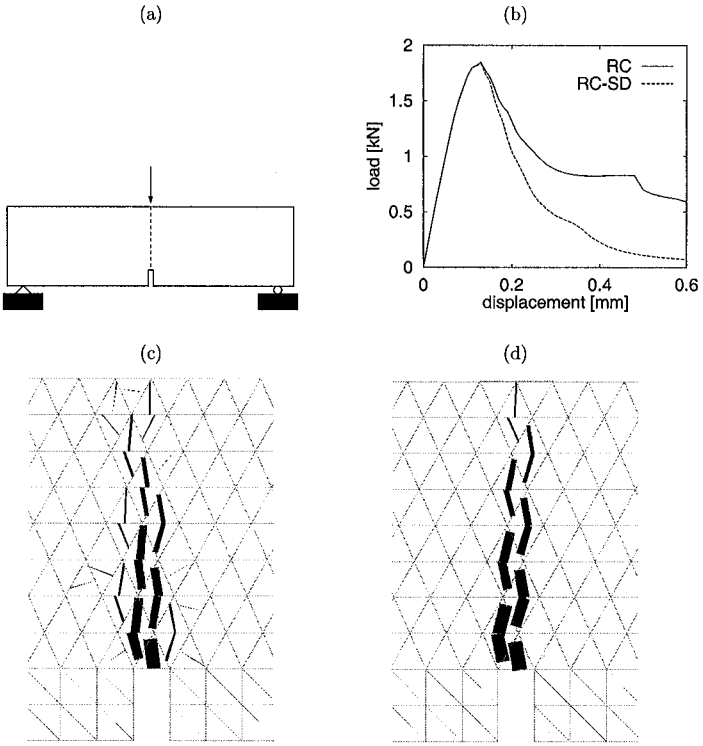

Figure 1. Three-point-bend specimen: (a) geometry and loading; (b) load–displacement diagrams; (c) crack pattern for standard elements and smeared rotating crack (RC) model; (d) crack pattern for standard elements and smeared rotating crack model with transition to scalar damage (RC-SD).

the results obtained with ordinary CST elements using, respectively, the standard rotating crack (RC) model [2] and the rotating crack model with transition to scalar damage (RC-SD), recently proposed by Jirásek and Zimmermann [3]. The dimensions and material parameters correspond to typical concrete fracture specimens; their exact values are not important, because the purpose of this example is to demonstrate certain pathological features that are of a general nature. As explained in Reference [4], unless the mesh is aligned such that the macroscopic crack can propagate in a band running parallel to the mesh lines (sides of finite elements), the RC model leads to severe stress locking. A typical consequence is an unrealistic load–displacement diagram with a non-negligible resisting force even at very late stages of the degradation process, when the crack should be almost completely stress-free. Spurious stresses transferred by the cracking band lead to additional cracking on both sides of the band and thus to an overestimated energy dissipation. The present type of locking can be alleviated by transition to a scalar damage model in those elements where the crack opening has reached a certain critical value. This is documented by the improved performance of the combined RC-SD model, for which the load–displacement diagram has a reasonable shape and cracking occurs only in one zig-zag layer of elements (see Figure 1(d)).

The problem has been re-analysed using the elements with embedded cracks described in Part I of this paper. As illustrated in Figure 2(a), the orientation of the discontinuity line predicted

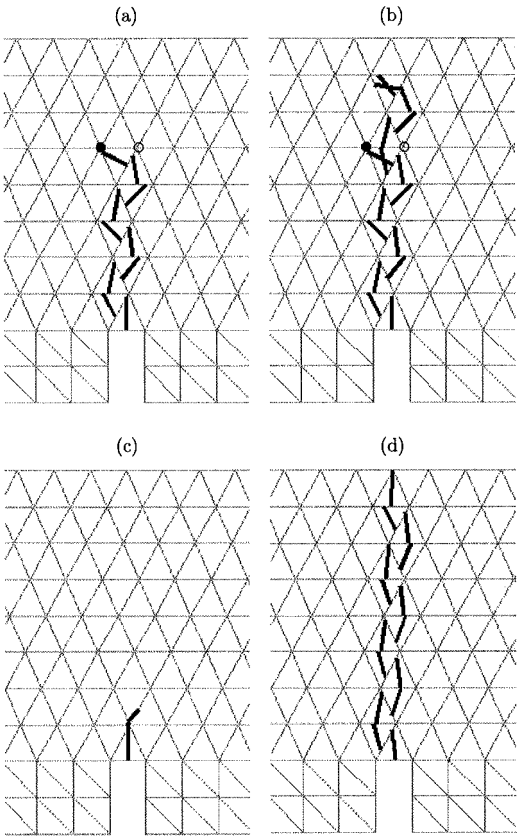

Figure 2. Evolution of crack pattern for a three-point-bend specimen: (a), (b) elements with embedded cracks (EC) and discontinuous crack path; (c) elements with embedded cracks (EC) and continuous crack path; (d) elements with delayed embedded cracks (DEC; to be described in Section 2).

from the local criterion of maximum principal stress is not always well aligned with the actual macroscopic crack.[§] Sometimes the embedded cracks fail to properly separate nodes that should be on the opposite sides of the band of cracking elements. This is the case for example for the topmost crack in Figure 2(a), which should (but does not) separate the nodes marked by circles. In a model with only one embedded discontinuity per element this leads to a severe locking because the macroscopic crack cannot open properly. It is therefore essential to allow the formation of another discontinuity line within the same element if the maximum principal stress exceeds the tensile strength and the rotation of the corresponding principal axis with respect to the primary discontinuity exceeds a certain threshold angle. If the primary embedded crack locks, the secondary one can release spurious stresses by correctly separating the nodes and allowing the propagation of the cracking band in the correct overall direction. Typically, the secondary discontinuity dominates

[§]In Figure 2, all lines representing embedded cracks have the same thickness, independent of the crack opening.

the failure process while the original one formed in a wrong direction either closes or at least does not open very fast. Figure 2(b) shows that the problem with incorrect separation of nodes may later reappear in another element.

When multiple cracking is allowed, the model can reproduce the overall fracture pattern in a satisfactory way. No excessive spurious stress transfer occurs, and the load–displacement diagram is very close to that obtained with the RC-SD model; see the curve with label embedded crack (EC) in Figure 3. However, the introduction of a secondary crack is (in the present context) only an artificial remedy—it relaxes the stress in a situation that would otherwise lead to locking. The secondary crack has nothing to do with the physical nature of the process because it appears only if the direction of the primary crack is mispredicted. Multiple cracking complicates the numerical algorithm and has an adverse effect on its robustness. Note that enforcement of a continuous crack path would not remedy the problem. In fact, in the present example the crack separating nodes incorrectly would appear even earlier (see Figure 2(c)).

2. DELAYED EMBEDDED CRACKS

2.1. Transition from smeared to embedded crack

The direction of an embedded discontinuity, once introduced, is normally kept fixed. Recently, some researchers have proposed models with rotating discontinuities [5–7]. It is questionable whether such formulations can lead to efficient and robust numerical algorithms. According to the present authors' experience, the passage of a node from one side of the discontinuity to the other generates numerical instabilities, and a special treatment is required to handle such situations. Also, some doubts have been raised regarding the thermodynamic admissibility of a rotating discontinuity. Nevertheless, this idea certainly deserves a further investigation.

In the present study we shall explore an alternative way of allowing an adjustment of the crack path. Observing the evolution of the crack pattern simulated with a smeared crack model, e.g. with the RC-SD model, we note that the initial misprediction of the crack direction is often corrected as the crack grows, because the overall evolution of the cracking band forces each individual crack to rotate into a position in which it separates nodes correctly (cf. Figure 1(d)). So it can be expected that the resolution of the macroscopic crack shall be improved if we do not introduce the displacement discontinuity immediately at the onset of cracking but we start with a smeared crack description and activate an embedded crack only after a certain critical crack opening, say w_t, has been reached. For easy reference, let us call such an approach the *delayed embedded crack model* (DEC), as opposed to the 'pure' embedded crack model (EC) with displacement discontinuities introduced right at the onset of cracking.

The DEC model can be described as a smeared crack model with transition to an embedded crack. At every material point, the initial stage of cracking is modeled in a smeared manner, i.e. in terms of cracking strain. When the crack opening (defined as the cracking strain multiplied by the effective element size [8, 9, 2]) reaches a critical value, a displacement discontinuity is introduced into the respective finite element. From that moment on, damage in the bulk of the material is frozen, and further degradation is described by damage at the embedded interface. This means that, after transition to the embedded crack, the bulk material is considered as linear elastic, however, with a material stiffness matrix that corresponds to the secant (unloading) stiffness of the smeared model at the time of transition. Of course, it is necessary to tune up the material parameters of

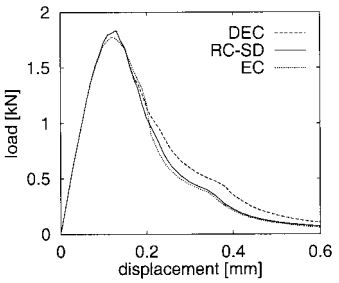

Figure 3. Load–displacement diagrams for the three-point-bend specimen. The curves have been obtained with the delayed embedded crack model (DEC), smeared rotating crack model with transition to scalar damage (RC-SD), and embedded crack model (EC).

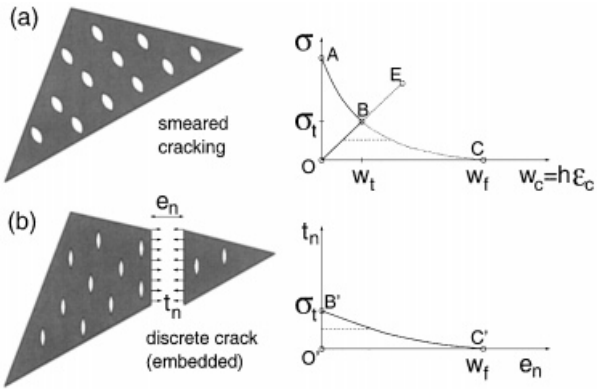

Figure 4. Matching of material laws for the smeared and discrete parts.

both components—the continuum law for the smeared part and the interface law for the discrete part—such that the transition is smooth and the total energy dissipation is correct.

The matching of the constitutive relations is illustrated in Figure 4. The diagram in Figure 4(a) corresponds to the stress–separation law exploited by the smeared model. To construct the stress–strain law, the crack opening, w_c, is transformed into the cracking strain, $\varepsilon_c = w_c/h$, where h is the effective element size. This is the usual technique applied in simulations of localization due to strain softening in order to avoid pathological sensitivity to the element size [8, 9]. A standard smeared crack model would follow the complete softening curve A–B–C; the area under this curve corresponds to the fracture energy of the material. The smeared part of a DEC model follows the initial part A–B of the softening curve, but at point B the diffuse damage is frozen, i.e. the smeared cracks are not allowed to grow anymore. The bulk of the material is now treated as linear elastic with a reduced stiffness, and the dependence between the smeared cracking strain and the stress normal to the cracks is described by the straight line O–B–E. At the same time, a discrete crack is embedded into the element, governed by the traction–separation law plotted in Figure 4(b). The softening curve B′–C′ is constructed as the difference between curve B–C and straight line B–O in the top diagram. Consequently, curved triangles OBC and O′B′C′ have exactly the same area, and the energy dissipated by the embedded crack is equal to the difference between the fracture energy (area of OABC) and the energy dissipated by the smeared crack (area of OAB). As the traction transmitted by the embedded crack decreases, the stress normal to the smeared crack must also decrease, and the smeared part of the model follows the segment B–O rather than B–E. Strictly speaking, all these considerations are exact only in the simple uniaxial case, but numerical experience shows that the results are reasonable even in more complex situations.

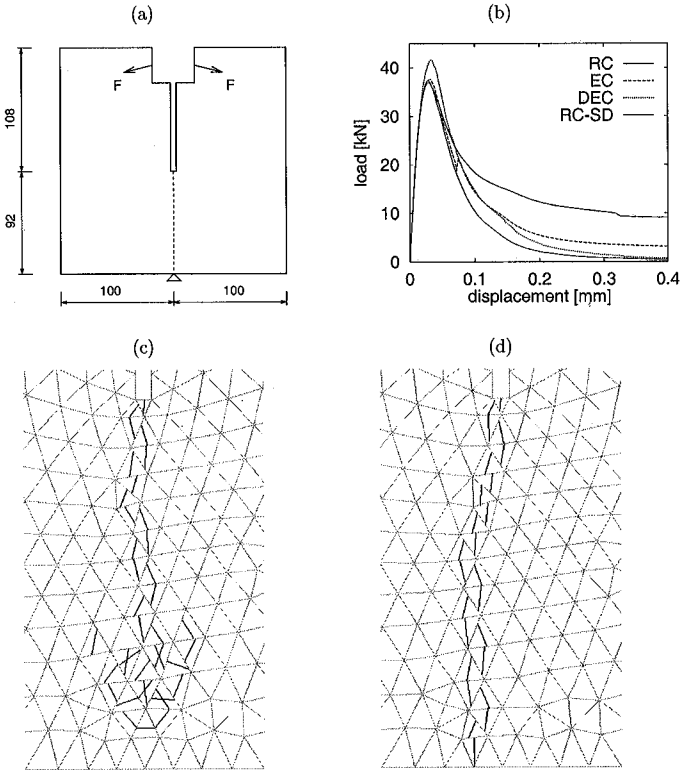

Figure 5. Wedge-splitting test: (a) specimen geometry and loading; (b) load–displacement diagrams; (c) crack pattern for elements with embedded cracks (EC); (d) crack pattern for elements with delayed embedded cracks (DEC).

2.2. *Results of simulations*

The crack pattern in Figure 2(d), obtained with the DEC model, indicates that the delay indeed leads to an improvement in the orientation of individual discontinuities. The complete failure pattern has formed without any secondary cracking, with a single crack per element. The load–displacement diagram in Figure 3 is very similar to those obtained with the RC-SD model and with the (multiple) EC model.

The simulations have been repeated for a wedge-splitting specimen tested by Slowik [10]. The material parameters for the smeared models (RC and RC-SD) have been taken from [3]: Young's modulus $E = 50\,\text{GPa}$, Poisson's ratio $\nu = 0.2$, tensile strength $f_t = 2.9\,\text{MPa}$, and fracture energy $G_f = 70\,\text{N/m}$. The embedded crack model has used the same basic properties and the same type of softening law (bilinear) as the smeared model. The ratio of reference stiffnesses D_{ss}/D_{nn} has been taken as 1, and for the DEC model transition took place at crack opening $w_t = 16\,\mu\text{m}$. Figure 5 shows the load–displacement diagrams for various models and the crack patterns for EC and DEC elements. Again, we observe that the embedded cracks alleviate stress locking, even though the EC model still gives a somewhat too stiff response in the late stages of softening. The DEC model leads to a more regular crack pattern with a less significant amount of secondary cracking.

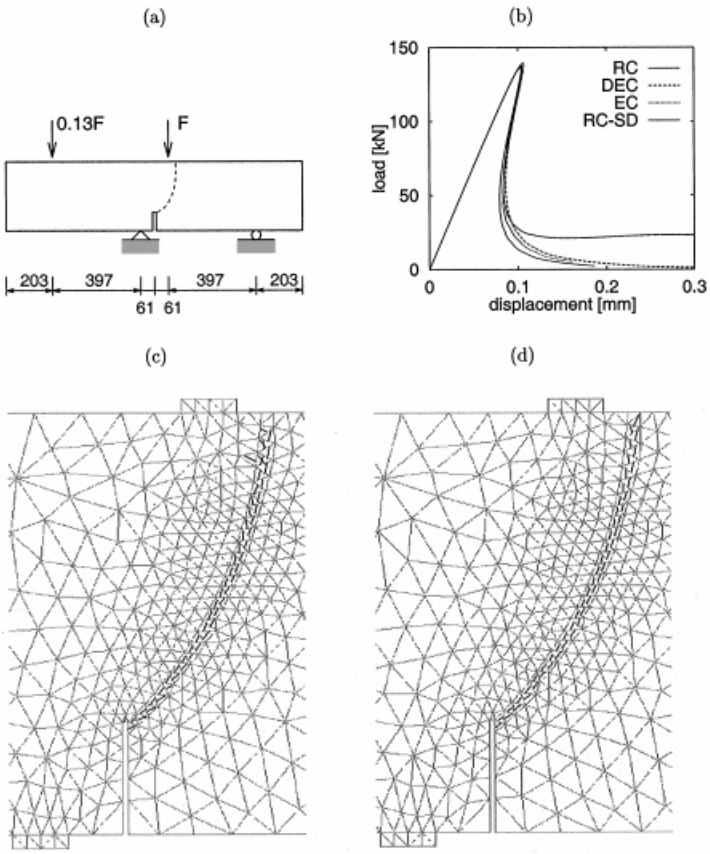

Figure 6. Four-point shear test: (a) specimen geometry and loading; (b) load–displacement diagrams; (c) crack pattern for elements with embedded cracks (EC); (d) crack pattern for elements with delayed embedded cracks (DEC).

Figure 6 shows the results of a simulation of the four-point shear specimen tested by Arrea and Ingraffea [11]. The material parameters for the smeared models (RC and RC-SD) have been taken from Reference [3]: $E = 30\,\text{GPa}$, $v = 0.18$, $f_t = 3.5\,\text{MPa}$, and fracture energy $G_f = 140\,\text{N/m}$. The embedded crack model has used the same basic properties. The ratio of reference stiffnesses D_{ss}/D_{nn} has been taken as 1, and for the DEC model transition took place at crack opening $w_t = 26.7\,\mu\text{m}$. In order to avoid troubles with mesh-induced directional bias we have used a mesh that offers the crack an opportunity to propagate through a layer of elements arranged along a smooth curve which approximately corresponds to the experimentally observed trajectory (dashed curve in Figure 6(a)). The load–displacement diagram in Figure 6(b) confirms that the embedded crack models do not exhibit locking even if the macroscopic crack trajectory is curved. The crack patterns are shown in Figures 6(c) and 6(d). The EC and DEC elements give almost identical results but convergence problems appear for the EC approach due to multiple cracking at late stages of the loading process. The DEC approach is more robust and allows to continue the simulation up to the formation of a complete crack.

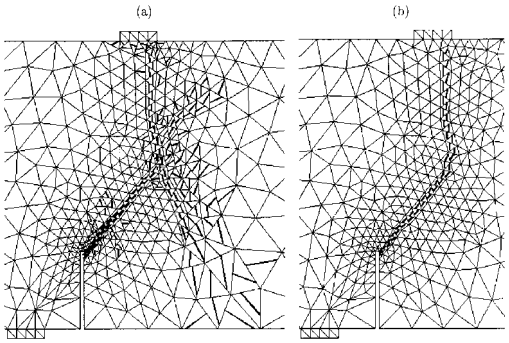

Figure 7. Four-point shear test simulated on a less favourable mesh: (a) crack pattern for standard elements and smeared rotating crack model (RC); (b) crack pattern for elements with delayed embedded cracks (DEC).

3. NON-LOCAL FORMULATION

3.1. Motivation

The model combining the embedded crack technique with the smeared crack approach reduces the amount of secondary cracking but still suffers by mesh-induced directional bias. This is illustrated in Figure 7, which shows the final crack patterns for the four-point shear test simulated on a less favourable mesh. In this case, the mesh was generated without taking into account the expected crack trajectory, and the crack band cannot propagate along a smooth curve. Initially, the band of cracking elements starts from the notch and follows the preferred mesh lines that are close to the correct direction. However, in the region where the mesh is not aligned with the actual crack trajectory, the computational crack is attracted by mesh lines running approximately in the vertical direction. For the standard rotating crack model (RC), this is accompanied by severe stress locking, because the initial branch has to open in a mixed mode, which is not correctly reproduced by the standard finite element kinematics. Due to locking, secondary cracking is produced and the cracking band develops additional branches that are clearly non-physical (Figure 7(a)). The DEC model, using the smeared rotating crack at early stages and explicitly modelled displacement discontinuity embedded into finite elements at late stages of the fracture process, does not suffer by locking and provides a clean cracking band (Figure 7(b)), but the direction of the band is obviously biased by the finite element mesh. Dependence of the crack trajectory on the orientation of mesh lines can be alleviated if the smeared part of the model is reformulated as non-local. In all examples below, the smeared part is represented by a non-local isotropic damage model.

3.2. Description of non-local model

The material law exploited here is a modified version of the non-local damage model proposed by Pijaudier-Cabot and Bažant [12]. The stress–strain law is written in the compact tensorial notation as

$$\boldsymbol{\sigma} = (1 - \omega)\mathbf{D}_e : \boldsymbol{\varepsilon} = (1 - \omega)\boldsymbol{\sigma}_e \tag{1}$$

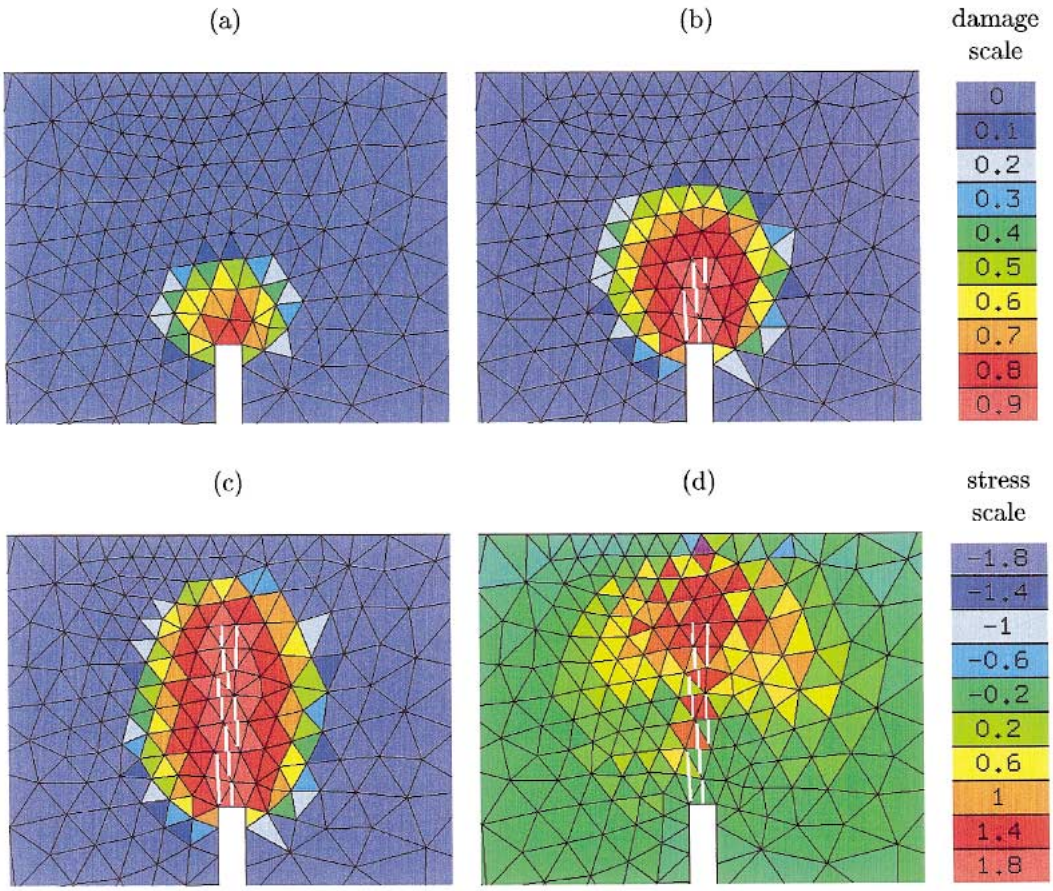

Plate 1. Three-point bending simulated by the non-local isotropic damage model with transition to embedded crack: (a)–(c) evolution of the fracture process zone; and (d) maximum principal stress.

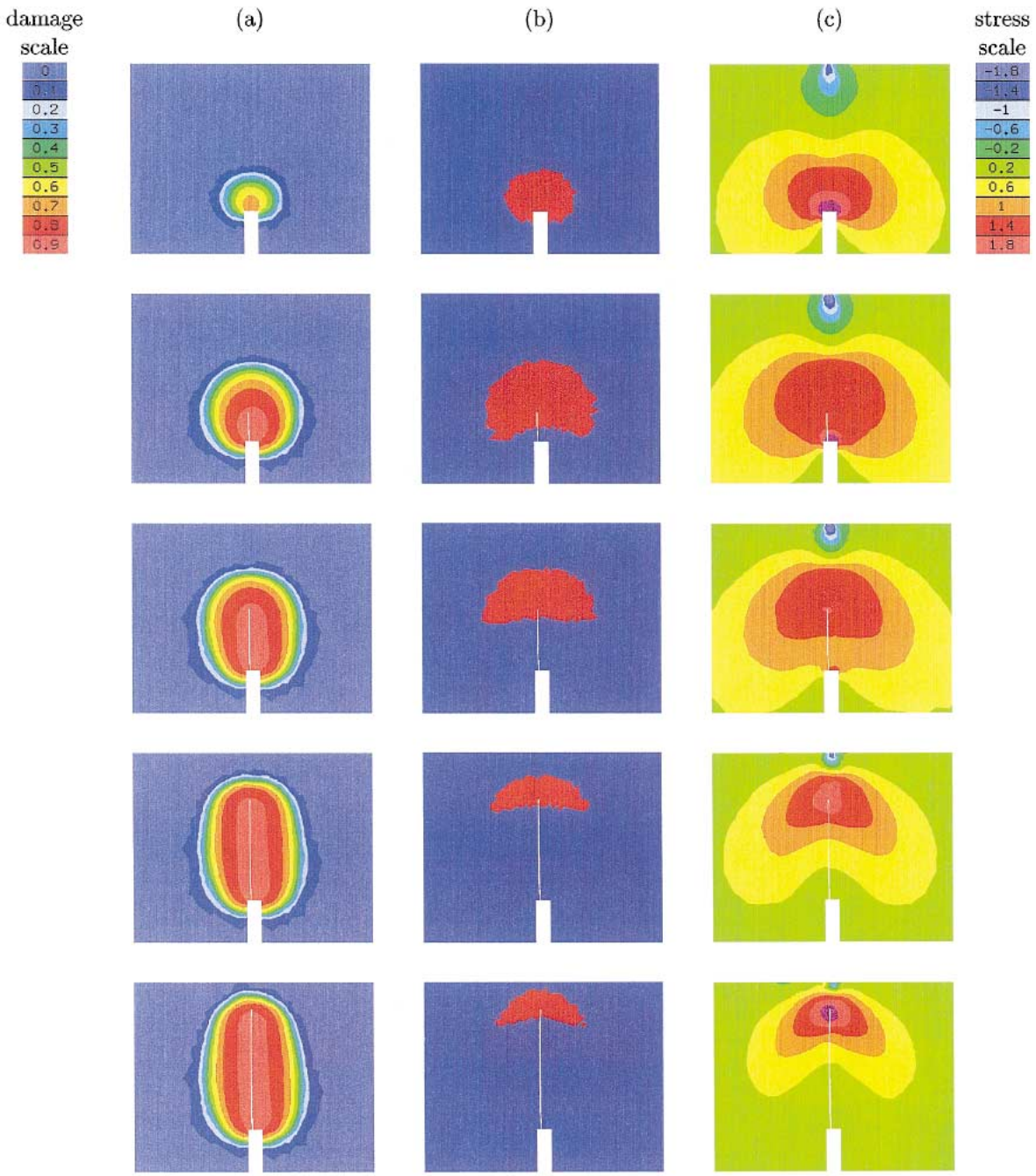

Plate 2. Evolution of the fracture process zone: (a) levels of damage; (b) region of growing damage; and (c) levels of maximum principal stress.

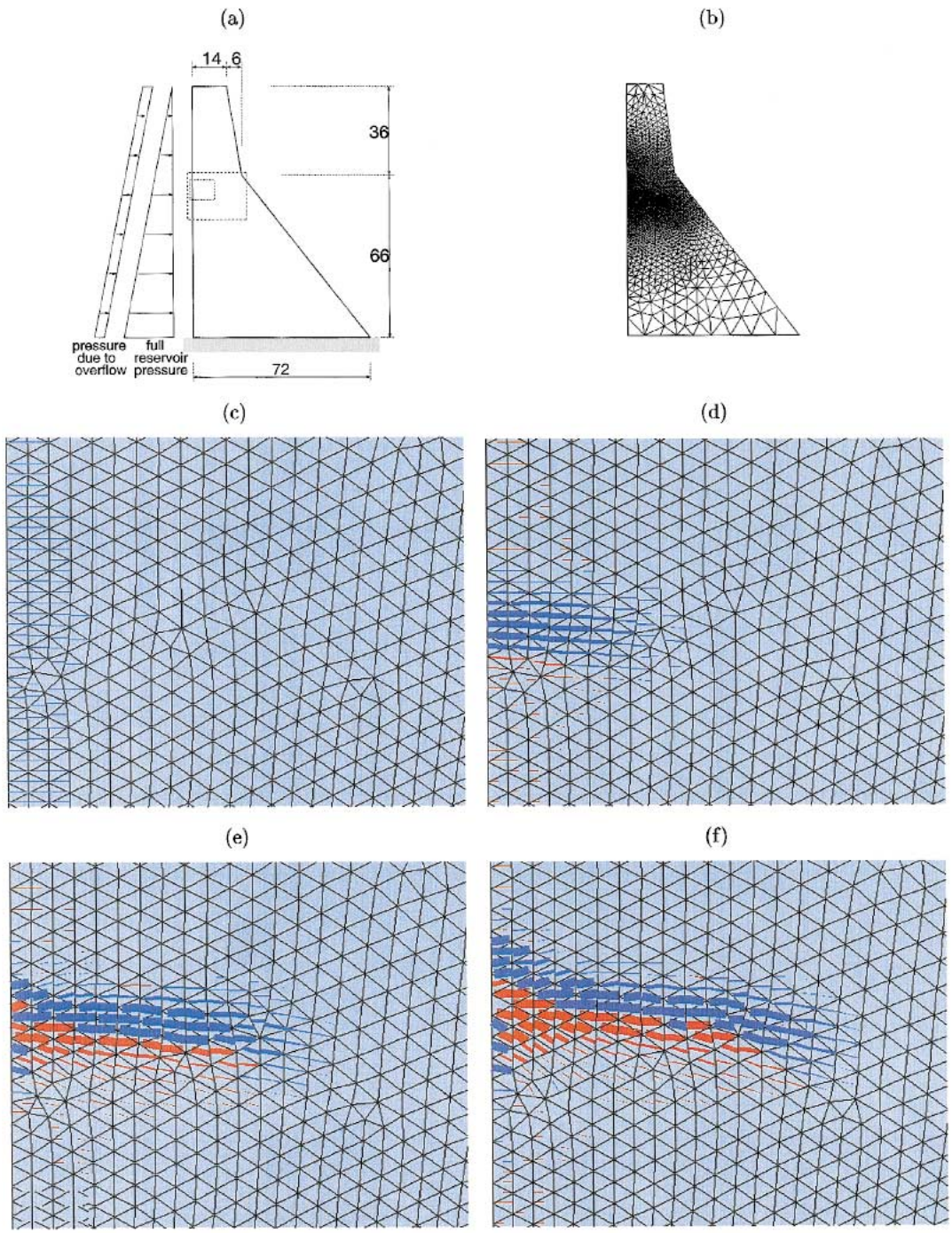

Plate 3. Analysis of a gravity dam: (a) geometry and loading; (b) finite element mesh; and (c)–(f) evolution of the crack pattern (close-up of the area marked in (a) by a dotted rectangle).

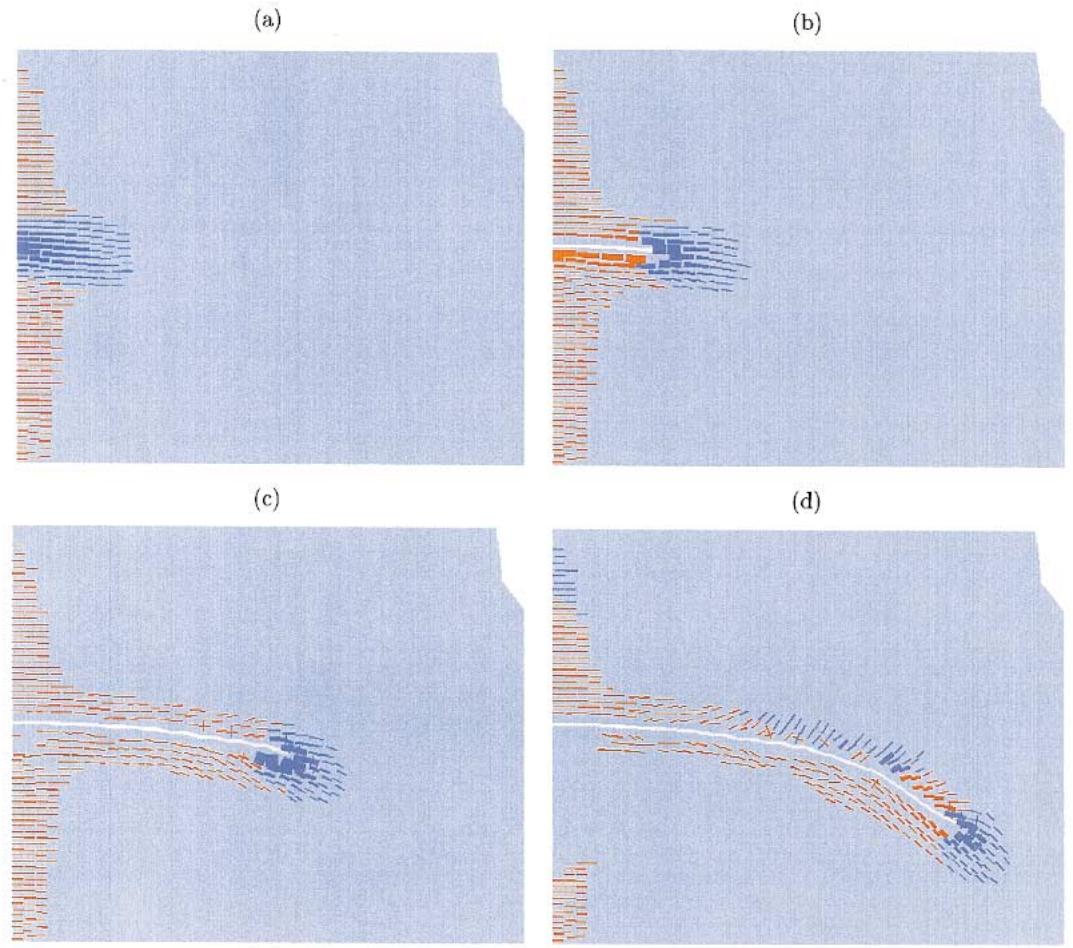

Plate 4. Fracture process zone development and propagation of a discrete crack modeled as a displacement discontinuity embedded in finite elements (close-up of the area marked in Plate 3(a) by a dashed rectangle).

where ω is a scalar damage parameter, and $\boldsymbol{\sigma}_e = \mathbf{D}_e : \boldsymbol{\varepsilon}$ is the effective stress. In Reference [12], the evolution of damage was controlled by the damage energy release rate, $Y = \boldsymbol{\varepsilon} : \mathbf{D}_e : \boldsymbol{\varepsilon}/2$. This basic version of the isotropic damage model is not appropriate for concrete, which has very different properties in tension and in compression. We restrict our attention to predominantly tensile failure and assume unlimited compressive strength. The evolution of damage is driven by the equivalent strain

$$\tilde{\varepsilon} = \frac{1}{E}\sqrt{\langle \boldsymbol{\sigma}_e \rangle : \langle \boldsymbol{\sigma}_e \rangle} \tag{2}$$

where the McAuley brackets $\langle \cdot \rangle$ denote the 'positive part' operator. For a scalar x, the positive part is defined as $\langle x \rangle = \max(0, x)$. For a symmetric second-order tensor $\boldsymbol{\sigma}$, the positive part is a tensor $\langle \boldsymbol{\sigma} \rangle$ with the same pricipal axes as $\boldsymbol{\sigma}$ and with principal values obtained by extracting the (scalar) positive part of the corresponding principal values of $\boldsymbol{\sigma}$.

Initially, the damage parameter is equal to zero, and the response of the material is linear elastic. When the equivalent strain reaches a certain threshold value, ε_0, the damage parameter starts growing, which reflects the gradual loss of integrity of the material. Due to the special choice of the expression for equivalent strain (2), the elastic domain in the principal stress space is similar to the one described by the Rankine criterion of maximum principal stress, with a smooth round-off of the edges and vertex corresponding to biaxial and triaxial tension. For general applications, covering also compressive failure, it would be necessary to refine the model, e.g. using the ideas from Reference [13].

During unloading, characterized by a decreasing value of $\tilde{\varepsilon}$, the damage parameter remains constant. This can be taken into account by making ω dependent on a softening parameter, $\tilde{\varepsilon}_{\max}$, which is defined as the maximum value of $\tilde{\varepsilon}$ reached in the previous history of the material up to the current state. The damage evolution is then described by the explicit relation

$$\omega = g_\omega(\tilde{\varepsilon}_{\max}) \tag{3}$$

and function g_ω can be identified from the uniaxial tensile stress–strain curve. Here we take a simple law [14]

$$\omega = g_\omega(\tilde{\varepsilon}_{\max}) \equiv \begin{cases} 0 & \text{if } \tilde{\varepsilon}_{\max} \leqslant \varepsilon_0 \\ 1 - \dfrac{\varepsilon_0}{\tilde{\varepsilon}_{\max}} \exp\left(-\dfrac{\tilde{\varepsilon}_{\max} - \varepsilon_0}{\varepsilon_{\mathrm{f}} - \varepsilon_0}\right) & \text{if } \tilde{\varepsilon}_{\max} \geqslant \varepsilon_0 \end{cases} \tag{4}$$

which corresponds to linear elastic behaviour up to the peak stress, $f_{\mathrm{t}} = E\varepsilon_0$, followed by exponential softening. The parameter ε_{f} affects ductility of the response and is related to the fracture energy of the material.

In the non-local version of the model, the 'local' equivalent strain, $\tilde{\varepsilon}$, is replaced by its weighted average over a certain neighbourhood of the given point,

$$\bar{\varepsilon}(\mathbf{x}) = \int_V \alpha(\mathbf{x}, \boldsymbol{\xi}) \tilde{\varepsilon}(\boldsymbol{\xi}) \, \mathrm{d}\boldsymbol{\xi} \tag{5}$$

The non-local weight function is usually defined as

$$\alpha(\mathbf{x}, \boldsymbol{\xi}) = \frac{\alpha_0(\|\mathbf{x} - \boldsymbol{\xi}\|)}{V(\mathbf{x})} \tag{6}$$

where

$$\alpha_0(r) = \begin{cases} \left(1 - \dfrac{r^2}{R^2}\right)^2 & \text{if } 0 \leqslant r \leqslant R \\ 0 & \text{if } R \leqslant r \end{cases} \tag{7}$$

is a bell-shaped function decaying with the distance $r = ||\mathbf{x} - \boldsymbol{\xi}||$ between points $\mathbf{x}$ and $\boldsymbol{\xi}$. For given $\mathbf{x}$, the support of $\alpha(\mathbf{x}, \boldsymbol{\xi})$ (i.e. closure of the set of points $\boldsymbol{\xi}$ at which $\alpha(\mathbf{x}, \boldsymbol{\xi})$ is non-zero) is a circle or sphere of radius R centered at $\mathbf{x}$. In (6), the scaling factor

$$V(\mathbf{x}) = \int_V \alpha_0(||\mathbf{x} - \boldsymbol{\xi}||)\, \mathrm{d}\boldsymbol{\xi} \tag{8}$$

ensures that the normalizing condition

$$\int_V \alpha(\mathbf{x}, \boldsymbol{\xi})\, \mathrm{d}\boldsymbol{\xi} = 1 \tag{9}$$

holds even in the vicinity of the boundary, where the support of $\alpha(\mathbf{x}, \boldsymbol{\xi})$ protrudes outside the domain V. Parameter R can be called the interaction radius because the non-local strain at a given point is affected only by points closer than R. The interaction radius is directly related to the non-local characteristic length of the material, which in turn depends on the microstructure, e.g. on the size and spacing of major inhomogeneities.

3.3. Simple simulations

Numerical simulations performed with the non-local delayed embedded crack model have revealed the importance of the criterion for placing the discontinuity line. The direction of the discontinuity line is assumed to be perpendicular to the direction of maximum principal stress or strain. However, the exact position of the discontinuity is not fully determined even when the direction is known. It is necessary to supply an additional piece of information, e.g. select one point of the discontinuity line. In principle, this could be any point of the corresponding finite element.

Consider first the case when the position of each embedded crack is determined by the element centre and when the crack is perpendicular to the direction of maximum principal stress (which coincides with the direction of maximum principal local strain) at the time of transition from smeared to embedded crack formulation. In this case, the crack segments in neighbouring elements in general do not form a continuous path. Plate 1(a)–(c) shows the evolution of the fracture process zone in a three-point-bend specimen from Figure 1(a). The mesh is somewhat finer than in the original example from Figure 1, to make sure that the non-local interaction is properly captured (the distance between neighbouring integration points must be smaller than the interaction radius of the non-local model). Only the opening embedded cracks are explicitly visualized as discontinuities (white lines) while the diffuse damage in the continuous part of the model is represented by the color scale.¶ Severe stress locking is observed at later stages of the loading process. This is

¶Note that Plate 1 displays the raw results directly obtained from the finite element interpolation. As the elements are constant strain triangles, the stress state and the damage parameter in each element are constant, with jumps between elements.

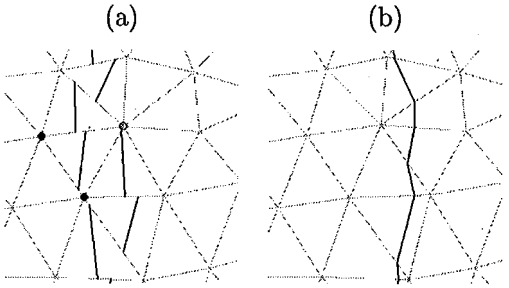

Figure 8. (a) Incorrect and (b) correct separation of nodes.

documented in Plate 1(d), which shows the distribution of the maximum principal stress in the state corresponding to Plate 1(c).

The source of locking is revealed in the close-up in Figure 8(a)— the embedded cracks do not separate the nodes correctly. The two nodes marked by filled circles are obviously on the same side of the band of cracking elements while the node marked by an empty circle is on the opposite side. However, the discontinuity line in the corresponding element fails to separate one of the filled circles from the empty circle, and the macroscopic crack cannot open properly. Paradoxically, the alleviation of mesh bias has rather an adverse effect. The smeared cracks do not rotate into a position in which they would separate the nodes correctly because they remain aligned with the macroscopic crack trajectory. The remedy is to enforce continuity of the embedded crack path. Instead of placing each discontinuity line into the centre of the corresponding element, it is checked whether one of the neighbouring elements already has an embedded discontinuity that intersects the common side. If this is the case, the new discontinuity line is placed such that it intersects the common side at the same point. Figure 8(b) demonstrates that this technique properly separates the nodes, so that the crack can open without any spurious stress transfer.

When continuity of the crack path is enforced, locking disappears and the overall crack direction is correct but locally the crack is tortuous; see Figure 9(a). Mesh refinement does not always help, as is clear from the bottom part of the figure. A perfectly straight crack trajectory in exactly the correct direction is obtained if the crack path continuity is enforced and if, in addition, the direction of the crack segment in each element is taken as orthogonal to the direction of maximum principal *non-local* strain; see Figure 9(b). The results are confirmed by simulation on a fine mesh with a clearly marked preferred direction deviating only slightly from the correct crack trajectory. The bottom part of Figure 9(b) demonstrates a remarkable insensitivity of the simulated trajectory to the orientation of the mesh.

The evolution of the fracture process zone and the gradual transition from a continuous representation of cracking to a discontinuous one is illustrated in Plate 2. The results shown in Plate 2(a), (c) have been postprocessed by a smoothing procedure. The colors correspond to various levels of total damage in the bulk of the material (Plate 2(a)) and of the maximum principal stress (Plate 2(c)). Plate 2(b) provides information on the increments of damage (not postprocessed). The red color indicates growing damage (non-zero increments) while the region where damage remains constant is plotted in blue. It is obvious that the bulk material in the wake of the embedded crack is unloading. Diffuse damage keeps growing in a limited region, which is situated mainly ahead of the embedded crack tip. In the remaining part of the fracture process zone, the damage parameter does not evolve anymore. The present model is therefore capable of

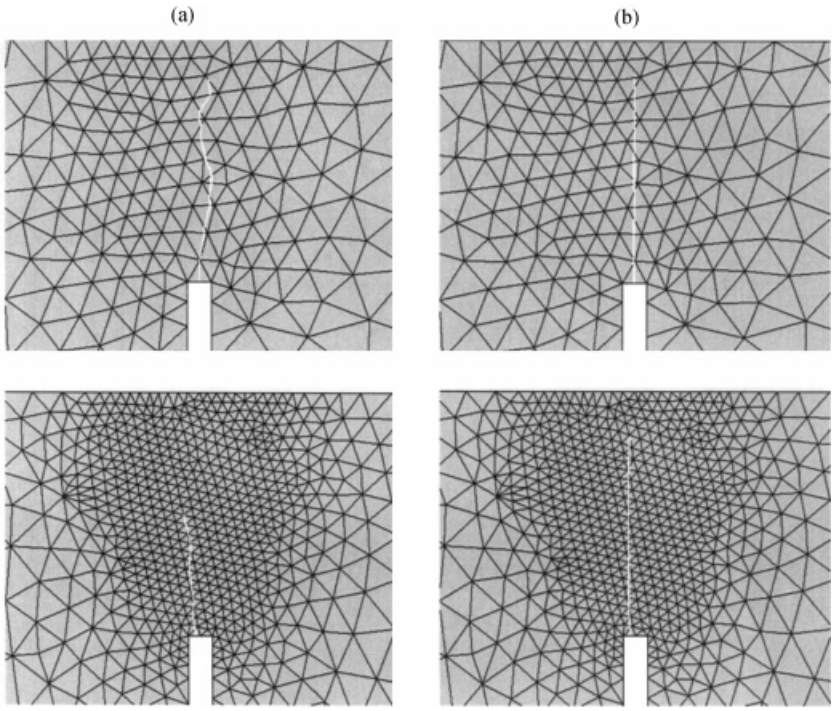

Figure 9. Embedded crack trajectory for a model with enforced continuity of the crack path, with direction determined: (a) from the local strain; (b) from the non-local strain.

describing the transition from diffuse to highly localized damage. Let us emphasize that, at any stage of the loading process, the model contains simultaneously a discrete crack (embedded in finite elements) and regions with growing and closing smeared cracks. This concept is more flexible and better reflects the actual physical processes than the approach previously proposed by Mazars and Pijaudier-Cabot [15, 16], which jumps from the continuum representation to the discrete one (or vice versa) at all material points simultaneously.

3.4. Application example

The preceding examples clearly demonstrate that the non-local formulation of the smeared part of the model substantially improves the insensitivity of the final embedded crack to the orientation of the finite element mesh. However, it is not clear yet whether the incorporation of embedded discontinuities into the combined model has also some beneficial effect on its overall performance. Originally, the embedded discontinuities were motivated by better resolution of the kinematics of a widely opening crack. Since stress locking does not seem to be a serious problem for non-local continuum models (unless it is induced by an inappropriate non-local formulation, see Reference [17]), one may be tempted to think that the transition to embedded cracks is only an elegant but dispensable addition to the conventional approach. However, there are a number of situations in which the improved representation of highly localized fracture is indeed essential. One of them

is described in the final example, while another has been discussed at a recent conference [18]. The growth and coalescence of microcracks in the fracture process zone eventually lead to the formation of a stress-free macroscopic crack. This is to some extent reflected by the evolution of the simulated process zone if the underlying model is based on non-local damage mechanics. In Reference [19] it was shown that the zone of increasing local strain gets thinner as the loading process continues, while the zone of increasing non-local strain keeps an approximately constant width. The secant material stiffness and the residual strength tend to zero in a finite zone whose thickness is equal to the support diameter of the non-local weight function (twice the interaction radius R). This zone must always contain several finite elements, otherwise the non-local interaction would not be properly captured by the numerical model. The complete degradation of the residual strength in a band containing several elements across its thickness is certainly not realistic and it causes serious numerical problems if the structure is subjected to distributed body forces. This is the case, e.g. in the analysis of gravity dams, where the effect of gravity forces is essential and cannot be neglected. The presence of gravity forces inside the fracture process zone leads to spurious shifting of the centre of the zone and finally to the divergence of the equilibrium iteration process, documented in Plate 3.

A gravity dam with dimensions corresponding to the well-known Koyna Dam (struck by an earthquake in 1967) is loaded by its own weight, full reservoir pressure, and an increasing hydrostatic pressure due to reservoir overflow (Plate 3(a)). The computational mesh, consisting of 4295 linear triangular elements, is shown in Plate 3(b). In a simulation using the non-local rotating crack model [3] with exponential softening and parameters $E = 25\,\mathrm{GPa}$, $\nu = 0.2$, $f_t = 1\,\mathrm{MPa}$, $\varepsilon_f = 300 \times 10^{-6}$, and $R = 1\,\mathrm{m}$, the initially diffuse cracking zone at the upstream face (Plate 3(c)) eventually localizes and propagates into the interior of the dam (Plate 3(d)). The close-up region depicted in Plate 3(c)–(f) is marked in Plate 3(a) by a small dotted rectangle. The larger dashed rectangle corresponds to the region that shall be shown in Plate 4. Blue and red rectangles represent opening and closing smeared cracks, respectively. When the mouth of the macroscopic crack opens sufficiently wide, the material becomes too weak to resist the (constant) body forces. The equivalent nodal forces start pulling down the nodes surrounded by the weakest material around the centre of the process zone, which closes the cracks in the bottom part of the zone and accelerates opening of the cracks in the top part. By non-local interaction, the opening cracks located close to the upper boundary of the process zone induce damage in the originally sane material layer located just above the process zone. By a domino effect, the active part of the zone travels upwards (Plate 3(e), (f)) until convergence is lost. Needless to say, this mechanism that shifts the numerical crack perpendicular to its trajectory is completely non-physical and has its origin in the assumption of a constant non-local interaction distance.

An elegant remedy is a gradual transition from a smeared to a discrete description of material failure. It can be argued that, as fracture progresses, long-range interaction between material points becomes more difficult and finally impossible. This would be best reflected by a non-local model with an evolving (decreasing) characteristic length. However, such a model would be computationally very expensive, since the interaction weights for all interacting pairs of integration points would have to be continuously recomputed. The approach proposed in the present paper can be considered as a reasonable approximation, with a constant interaction radius at low levels of damage and a discrete crack description (corresponding to a zero interaction radius) at high levels of damage.

The simulation of a gravity dam has been repeated using the model with transition from non-local rotating cracks to embedded displacement discontinuities (discrete cracks). The transition

takes place when the cracking strain reaches a certain critical value, in the present example taken as 500×10^{-6}, and the softening laws describing the smeared and discrete parts of the model are matched such that a smooth transition and correct energy dissipation are ensured. The initial cracking pattern is the same as before, but soon after localization the first discrete crack appears and propagates along the center of the fracture process zone (see the white curve in Plate 4). The partially damaged material in the wake of the discrete crack unloads, and its residual strength does not diminish anymore. Therefore, the correct crack trajectory can be captured without any numerical instabilities.

Note that the material in the wake of the embedded crack is in general unloading, because the traction carried by the discontinuity is relieved as the displacement jump increases. However, a cluster of active (opening) smeared cracks far behind the tip of the discrete crack can be detected in Plate 4(d). This is not a spurious effect produced by stress locking, but a natural indication of incipient branching of the primary macroscopic crack. This phenomenon has already been observed in simulations using a pure non-local rotating crack model [20] and has also been discussed and illustrated in Reference [21, p. 375 and front cover].

4. CONCLUDING REMARKS

Numerical testing has revealed that the conventional embedded crack approach, which introduces a displacement discontinuity right at the onset of cracking, often leads to a misprediction of the discontinuity direction. As the direction has to remain fixed, there is no chance for its adjustment. This inevitably leads to stress locking that must be relaxed by a secondary crack in the same element. Multiple cracking complicates the numerical algorithm and can lead to convergence problems. It has therefore been proposed to use a combined model that represents the early stage of cracking in a smeared manner and introduces a discontinuity only when the crack opens sufficiently wide. If the smeared part is modeled by the rotating crack approach, the crack has a chance to readjust its direction, and there is no need for secondary cracking. The combination of the smeared and embedded descriptions of cracking is appealing from the physical point of view. It is intuitively clear that diffuse damage at early stages of material degradation is adequately described by a model dealing with inelastic strain, while highly localized fracture is better represented by a displacement discontinuity. Examples of simulations of fracture specimens demonstrate the potential of the developed technique.

As an additional improvement, the smeared part of the combined model has been reformulated as non-local. It turns out that for the alleviation of locking it is essential to enforce continuity of the embedded crack trajectory. Optimal performance in terms of insensitivity to mesh-induced directional bias is obtained if the orientation of the embedded crack is in each element determined from the principal directions of non-local (rather than local) strain. Transition to the explicit description of a crack as a displacement discontinuity turns out to be an efficient remedy to pathological shifting of the process zone, exhibited by the non-local damage model with a constant characteristic length.

To summarize, the embedded crack approach seems to be a very appealing technique that certainly has a number of important advantages compared to more traditional approaches. Of course, a large amount of work still remains to be done. For example, a challenging goal would be an extension of the model to three dimensions.

ACKNOWLEDGEMENTS

Financial support of the Swiss Commission for Technology and Innovation under project CTI.3201.1 is gratefully acknowledged.

REFERENCES

1. Jirásek M, Zimmermann Th. Embedded crack model: I. Basic formulation. *International Journal for Numerical Methods in Engineering*, this issue.
2. Rots JG. Computational modeling of concrete fracture. *Ph.D. Thesis*, Delft University of Technology, Delft, The Netherlands, 1988.
3. Jirásek M, Zimmermann Th. Rotating crack model with transition to scalar damage. *Journal of Engineering Mechanics* ASCE 1998; **124**:277–284.
4. Jirásek M, Zimmermann Th. Analysis of rotating crack model. *Journal of Engineering Mechanics* ASCE 1998; **124**: 842–851.
5. Tano R. Localization modelling with inner softening band finite elements. *Licentiate Thesis*, Luleå University of Technology, Sweden, August, 1997; 26.
6. Tano R, Klisinski M, Olofsson Th. Stress locking in the inner softening band method: a study of the origin and how to reduce the effects. In *Computational Modelling of Concrete Structures*, de Borst R, Bićanić N, Mang H, Meschke G (eds). Balkema: Rotterdam, 1998; 329–335.
7. Sluys LJ, Berends AH. 2D/3D modelling of crack propagation with embedded discontinuity elements. In: *Computational Modelling of Concrete Structures*, de Borst R, Bićanić N, Mang H, Meschke G (eds). Balkema: Rotterdam, 1998; 399–408.
8. Pietruszczak S, Mróz Z. Finite element analysis of deformation of strain-softening materials. *International Journal for Numerical Methods in Engineering* 1981; **17**:327–334.
9. Bažant ZP, Oh BH. Crack band theory for fracture of concrete. *Matériaux et Constructions* 1983; **16**:155–177.
10. Slowik V. Beiträge zur experimentellen Bestimmung bruchmechanischer Materialparameter von Beton. *Building Materials Reports No.* 3, ETH Zürich, 1995.
11. Arrea M, Ingraffea AR. Mixed-mode crack propagation in mortar and concrete. *Department of Structural Engineering Report* 81-13, Cornell University, Ithaca, NY, 1981.
12. Pijaudier-Cabot G, Bažant ZP. Nonlocal damage theory. *Journal of Engineering Mechanics* ASCE 1987; **113**: 1512–1533.
13. Saouridis C, Mazars J. Prediction of the failure and size effect in concrete via a bi-scale damage approach. *Engineering Computations* 1992; **9**:329–344.
14. Oliver J, Cervera M, Oller S, Lubliner J. Isotropic damage models and smeared crack analysis of concrete. In *Computer Aided Analysis and Design of Concrete Structures*, Bićanić N, Mang H (eds). Pineridge Press: Swansea, UK, 1990; 945–957.
15. Mazars J, Pijaudier-Cabot G. From damage to fracture mechanics and conversely: a combined approach. *International Journal of Solids and Structures* 1996; **33**:3327–3342.
16. Bodé L, Tailhan JL, Pijaudier-Cabot G, La Borderie Ch, Clément JL. Failure analysis of initially cracked concrete structures. *Journal of Engineering Mechanics* ASCE 1997; **123**:1153–1160.
17. Jirásek M. Nonlocal models for damage and fracture: comparison of approaches. *International Journal of Solids and Structures* 1998; **35**:4133–4145.
18. Jirásek, M. Nonlocal damage models: practical aspects and open issues. *Proceedings of the 13th ASCE Engineering Mechanics Division Specialty Conference*, Johns Hopkins University, Baltimore, 13–16 June 1999. (CD-ROM)
19. Jirásek, M. Comparison of nonlocal models for damage and fracture. *LSC Internal Report* 98/02, Swiss Federal Institute of Technology at Lausanne, Switzerland, 1998.
20. Jirásek M, Zimmermann T. Rotating crack model with transition to scalar damage: I. Local formulation, II. Nonlocal formulation and adaptivity. *LSC Internal Report* 97/01, Swiss Federal Institute of Technology at Lausanne, Switzerland, 1997.
21. Bažant ZP, Planas J. *Fracture and Size Effect in Concrete and Other Quasibrittle Materials*. CRC Press: Boca Raton, 1998.

